JGR Oceans

RESEARCH ARTICLE
10.1029/2025JC023075

Regionalization and Multidecadal Change in the Southern Canary Current Large Marine Ecosystem

Juncal Cabrera-Busto[1], Eduardo Ramírez-Romero[1,2], Lucie Buttay[3,4], and Marcos Llope[5]

[1]Centro Oceanográfico de Cádiz (COCAD), Instituto Español de Oceanografía (IEO-CSIC), Cádiz, Spain, [2]Department of Ecology and Geology, Faculty of Sciences, University of Malaga, Málaga, Spain, [3]Institute of Marine Research (IMR), Tromsø, Norway, [4]Faculty of Biosciences, Fisheries and Economics, UiT—the Arctic University of Normay, Tromsø, Norway, [5]Centro Oceanográfico de Gijón/Xixón (COG), Instituto Español de Oceanografía (IEO-CSIC), Gijón/Xixón, Spain

Key Points:

- The Canary Current is divided into four subregions, although the exact boundaries vary among methodologies
- North Morocco upwelling became permanent, resembling the Western Sahara pattern
- The tropical subregion shows a warming trend and shorter upwelling periods

Supporting Information:

Supporting Information may be found in the online version of this article.

Correspondence to:

J. Cabrera-Busto and E. Ramírez-Romero, juncalcabrera@gmail.com; e.ramirez.romero@uma.es

Citation:

Cabrera-Busto, J., Ramírez-Romero, E., Buttay, L., & Llope, M. (2026). Regionalization and multidecadal change in the southern Canary Current Large Marine Ecosystem. *Journal of Geophysical Research: Oceans*, *131*, e2025JC023075. https://doi.org/10.1029/2025JC023075

Received 25 JUN 2025
Accepted 17 APR 2026

Author Contributions:

Conceptualization: Eduardo Ramírez-Romero, Marcos Llope
Formal analysis: Juncal Cabrera-Busto
Methodology: Juncal Cabrera-Busto, Eduardo Ramírez-Romero, Lucie Buttay
Writing – original draft: Juncal Cabrera-Busto
Writing – review & editing: Eduardo Ramírez-Romero, Lucie Buttay, Marcos Llope

Abstract The current delineation of the southern Canary Current Large Marine Ecosystem fisheries management zones responds only to political divisions rather than ecological features or a combination of both. In this paper, we implemented three time series analysis techniques on spatially explicit daily and monthly resolved data sets from satellite and reanalysis. Methods are based on climatologies, wavelet analysis and clusters and seasonal regression models, thus covering different aspects of the upwelling dynamics. Due to the overall convergence of the outputs of the analysis, by describing the spatiotemporal dynamics of oceanographic processes and biogeochemical features, we delineate distinct robust subregions and examine their recent trends. Our results identified four subregions: (a) a tropical subregion (12–18–21°N), (b) a Western Sahara (18–21°N to 25°N), (c) a South Morocco (26–28°N) and (d) a North Morocco subregion (29–35°N). The tropical subregion continues to exhibit a highly seasonal upwelling pattern with decreasing duration of winter upwelling events, in contrast with the other subregions that show slight variations in their seasonality. Although wind-driven upwelling has intensified in Western Sahara, leading to a cooling trend in sea surface temperature, chlorophyll-a does not show a concomitant increase. The North Morocco subregion is experiencing an increase in both the intensity and duration of the upwelling, making it more closely resemble the permanent upwelling zone of Western Sahara. This revisited subdivision provides a robust framework for ecosystem-based management by incorporating current ecological variability. Monitoring of hydrographic and biological trends is essential to adapt boundaries to future conditions.

Plain Language Summary Fisheries in the southern part of the Canary Current region are currently managed based on political borders rather than on how the ocean and marine ecosystems actually behave. However, ignoring the link between the environment and fish populations could undermine both conservation and fishing efforts. In our study, we analyzed decades of ocean data from satellites and models to understand how oceanographic patterns vary latitudinally across the region. Based on this, we identified four ecologically distinct subregions: Tropical, Western Sahara, South Morocco, and North Morocco. Each subregion shows unique oceanographic conditions and trends in key variables such as sea surface temperature, chlorophyll-a concentrations, and the timing and intensity of upwelling. Notably, variations in these factors across the four zones could have significant implications for the distribution and productivity of fish populations. These new boundaries offer a more accurate reflection of how the ocean operates and provide a foundation for more effective, flexible fisheries management. Permanent monitoring of these changing conditions will be essential for adapting to future environmental shifts and ensuring the sustainability of marine resources in the region.

1. Introduction

Eastern Boundary Upwelling Systems (EBUS) are areas of high primary productivity that support vast and diverse marine populations. With a combined surface area of less than 3% of the world's oceans, EBUS contributes to 20% of global fisheries and constitutes essential habitats for marine biodiversity (Pauly & Christensen, 1995). Over the past 60 years, three of the four major EBUS (California, Humboldt, and Benguela systems) have experienced significant wind intensification, whereas no such trend has been detected in the Canary Current (Bindoff et al., 2019). Despite the relatively high confidence in these wind observations, the implications for the resulting upwelling intensity remain uncertain (Bindoff et al., 2019) and observed changes exhibit substantial variability among and within EBUS (Bograd et al., 2023). For example, in the Canary Current, some

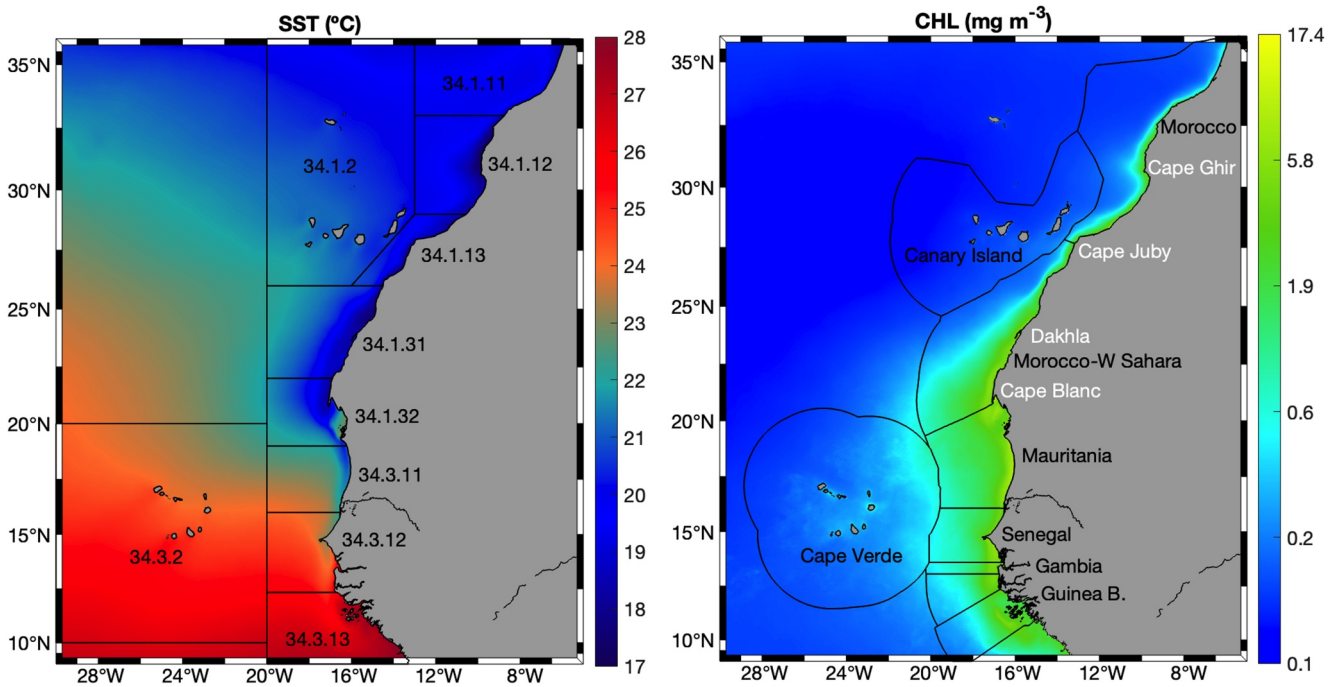

Figure 1. Study area. The left panel depicts the mean climatology of sea surface temperature (SST, °C) from 1982 to 2020 from CMEMS (Table S1 in Supporting Information S1), accompanied by the delineation of FAO fisheries areas (Table S2 in Supporting Information S1). The right panel illustrates the mean climatology of chlorophyll-a (CHL, mg m^{-3}) from 1998 to 2020 from CMEMS (Table S1 in Supporting Information S1), along with the demarcation of Exclusive Economic Zones (EEZ) for the countries.

studies identify intensified upwelling (e.g., Marcello et al., 2011; McGregor et al., 2007), while others report weakening or spatially contrasting patterns (Cropper et al., 2014; Gómez-Gesteira et al., 2008; Pardo et al., 2011; Wang et al., 2015).

The Canary Current Large Marine Ecosystem (CCLME) is the largest of the world's four major EBUS (Arístegui et al., 2009; Barton, 1998) and the second to third in terms of primary productivity (Chavez & Messié, 2009). This ecosystem presents great economic and social importance to the coastal populations and states of West Africa, providing sustainable livelihoods, fish-protein supplies and revenue to the region (Diogoul et al., 2021) and beyond (European Commission, 2023). The southern part of the CCLME (Figure 1) exhibits contrasted geographical and environmental features. Variability in coastline orientation, freshwater input, water masses dominance, wind stress, and dust deposition all contribute to this spatial heterogeneity (Arístegui et al., 2009; Cropper et al., 2014). In addition, mesoscale and submesoscale dynamical features, including eddies and filaments, play a key role in structuring the physical and biogeochemical variability of the system by modulating horizontal and vertical transport processes. Regarding the water masses distributions, the southern part, extending from Cape Blanc to Guinea-Bissau (10–21°N), is dominated by South Atlantic Central Waters (SACW), which are characterized by higher nutrient concentrations than the North Atlantic Central Waters (NACW). The NACW-dominated area extends northward from Cape Blanc to Morocco (21–35°N) (Gómez-Letona et al., 2017). In addition, due to its proximity to the Sahara desert, the CCLME experiences significant dust deposition, particularly in its southernmost regions, making it one of the world's most heavily affected areas by atmospheric fertilization process (Mahowald et al., 2005).

The current delineation of fisheries management zones in the southernmost area largely follows political boundaries, which may not align with the ecosystem's physical and biogeochemical characteristics driving species distribution. Species distributions are also expected to respond to ocean warming and environmental variability (Baudron et al., 2020; Pinsky et al., 2013). For example, changes in wind-driven upwelling intensity and seasonality can influence nutrient supply, primary productivity and habitat suitability. Although several studies have proposed alternative regionalizations based on physical and biogeochemical criteria, including upwelling seasonality and water mass characteristics (Arístegui et al., 2009; Cropper et al., 2014; Sylla et al., 2019, 2022;

Vázquez et al., 2022, 2023, 2024), these frameworks have not been incorporated into current fisheries management schemes. However, these studies overlook long-term trends or changes in seasonal dynamics observed over recent decades, leaving critical gaps in our understanding of how the system evolves in response to climate variability.

In this study, we aim to delineate physically and biogeochemically coherent subregions across the latitudinal extent of the southern CCLME, integrating atmospheric forcing (wind-driven upwelling), ocean dynamics (sea surface temperature), and biogeochemical properties (chlorophyll-a and dust deposition). Particular emphasis is placed on long-term trends and seasonal changes over recent decades, which were analyzed using three different time-series analysis methods.

This integrated regionalization provides a framework for interpreting ecosystem variability and supports the development of ecosystem-based fisheries management strategies in the region.

2. Methodology

2.1. Area of Study

The focus of the present study is the southern Canary Current Large Marine Ecosystem (sCCLME), extending from Morocco to Guinea-Bissau (12–35°N; Figure 1).

2.2. Data

Multiple data sources were gathered ad hoc for this study (Table S1 in Supporting Information S1). Namely, we extracted or computed the upwelling index (UI), sea surface temperature (SST), chlorophyll a (Chl) and dust deposition (dust). We processed the data in two formats:

1. coastal time series analysis, encompassing the variables averaged from the coastline up to 1° offshore and discretized for each latitude degree (24 series) (red line in Figure 3). Monthly averaged data were used for all time-series analyses, except for the wavelets analyze that was performed on daily time series of the upwelling index.
2. Monthly data rasters with higher spatial resolution.

A schematic representation of the methodology process is represented in Figure 2.

To evaluate how the segmentation of time series affects the estimated trends, we analyzed the time series both in their full available length (e.g., upwelling from 1967) and in the overlapping period available time series (1998–2020). This approach was motivated by findings from Sydeman et al. (2014), who conducted a meta-analysis of 22 studies (comprising 187 non-independent time series) across all four Eastern Boundary Upwelling Systems (EBUSs) and demonstrated that the length of time series has a significant impact on trend results. It also reflects the recommendations of Barton et al. (2013) and WMO (1996, 2007, 2017) to use periods longer than 30 years to mitigate biases associated with shorter time frames. To further assess the influence of the Atlantic Multidecadal Oscillation (AMO) on this variability, we selected an overlapping time period spanning from 1998 to 2020. This overlapping period aligns with the AMO phase change, as described later, and ensures consistency across variables, particularly chlorophyll and primary production data.

2.2.1. Bakun Upwelling Index

The Bakun (1973, 1975) upwelling index (UI^W) was calculated on monthly and daily data. To compute this, we used the angle of the coast and the components of offshore Ekman (Table S1 in Supporting Information S1), extracted at 1° (100 km) from the coast. UI^W is based on Ekman's theory of mass transport due to wind stress. Note that the calculation of Ekman transport utilizes a geostrophic approximation that is not valid close to the equator. For this reason, the analysis begins at 12°N, excluding areas to the south. Furthermore, to ensure UI^W patterns are not dependent on the resolution of the analyzed database, offshore wind-driven Ekman transport and UI^W were calculated from the ERA5 database (Table S1 in Supporting Information S1) following Gomez-Gesteira et al. (2006) and Sousa et al. (2017). The results were interpolated to match the same 1° grid of the NOAA database (Table S1 in Supporting Information S1).

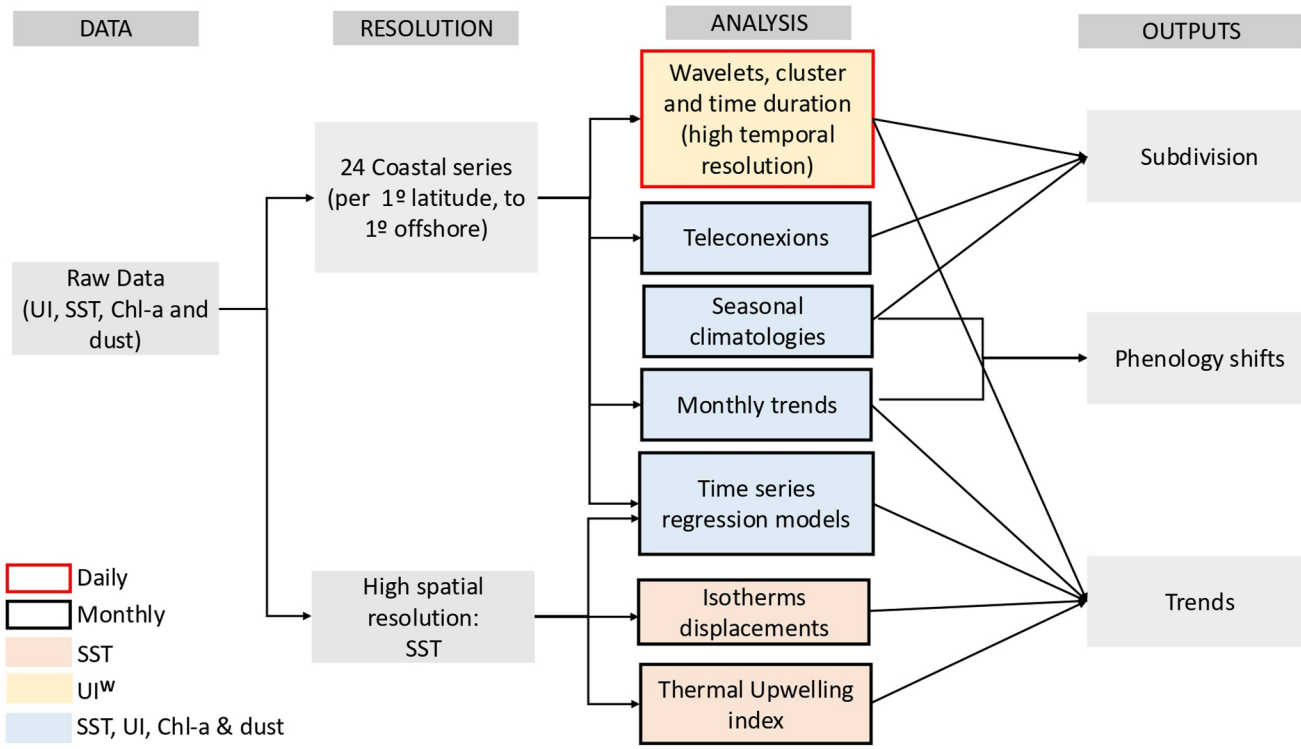

Figure 2. Scheme of the methodology used. Data were separated for two analyses: a coastal series analysis, where variable values were computed as the average from the coastline to up to 1° offshore and discretized for each latitude (1° resolution) and a high spatial resolution analysis, where the SST values are used at the highest spatial resolution available, analyzing time series at each grid point. Various analyses were conducted on this data set as outlined in the scheme. In the graph the yellow rectangle represents analysis where only UI^W data are used, orange rectangles analysis where only SST data are used, and blue rectangles analysis were all variables data are used. The contour of the rectangles represents the time resolution. Red contour means daily data, whereas black contours mean monthly data.

2.3. Statistical Analysis

2.3.1. Seasonal Climatologies

Climatologies were calculated to describe the seasonal patterns of UI^W, SST, Chl and dust at each latitude along the entire area. The seasonal cycle for each variable and latitude was calculated as the monthly average over the whole available period (see Table S1 in Supporting Information S1).

2.3.2. Wavelet Analyses

To identify regions of homogeneous upwelling dynamics, we conducted a wavelet transformation of each time series of UI^W (using daily data for each latitude from 1978 to 2020) and compared their time-frequency characteristics. Since upwelling plays a central role in this area, our wavelet analysis was performed exclusively on this variable, which constituted the longest time series available.

Wavelet transformation performs a local time-scale decomposition of the variance of the signal and allows, therefore, coping with the non-stationary behavior of the series (Cazelles et al., 2008). We used the Morlet wavelet, a continuous and complex function that enables the extraction of time-dependent amplitude cycles and whose scales are related to frequencies (Cazelles et al., 2008; Ménard et al., 2007). The resulting local Wavelet Power Spectrum (WPS) displays the relative importance of frequencies for each time step. Significance levels (5%) for WPS were determined through a bootstrapping scheme that used the hidden Markov model (Cazelles & Stone, 2003). To compare the dynamics between the series across the latitudinal gradient, we calculated the dissimilarity between the local WPS of each latitude based on the maximum correlation analysis method (Bretherton et al., 1992; Rouyer et al., 2008). For this purpose, singular value decomposition was performed on

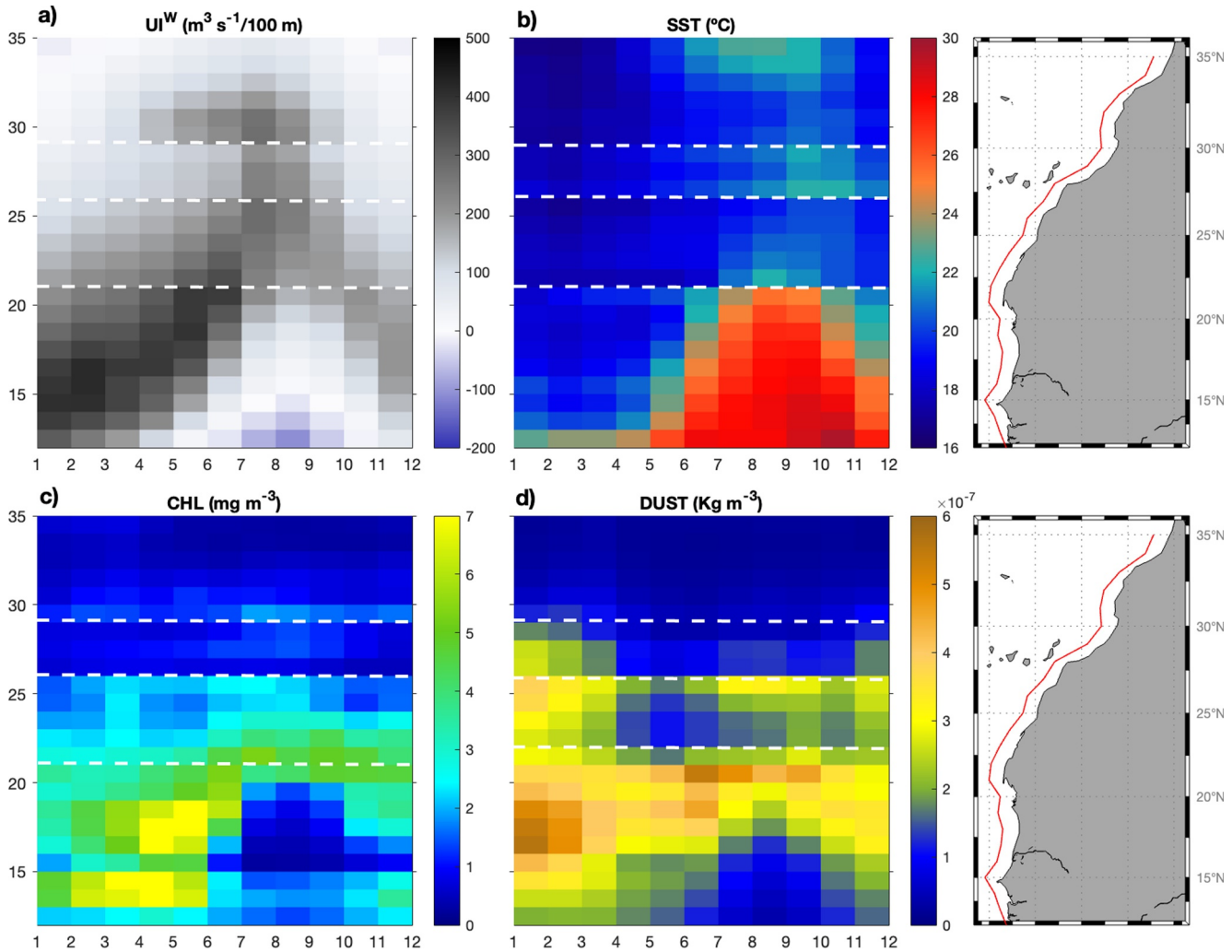

Figure 3. Climatologies. Panel (a) Bakun upwelling index (UI^W, $m^3 s^{-1}$/100 m) from NOAA (b) surface sea temperature (SST, °C), (c) chlorophyll-a (CHL, mg m^{-3}), and (d) dust concentration (kg m^{-3}). The values are obtained as the variable average from the coastline to up to 1° offshore (red line in the right maps) and discretized for each latitude. White dashed lines indicate the different subregions detected with this method.

the covariance matrix between two local WPS. The distance between each spectrum singular value, obtained in a diagonal matrix, was therefore represented in a dendrogram using Ward's (1963) method for clustering.

2.3.3. Trends Assessments

A time series regression model was fitted to separate the variability of the series into a seasonal component, a (linear) long-term trend and a noise component, as described by Llope et al. (2007) (Equation 1).

$$Y_t = a + b_t + c_1\,\mathrm{Jan}_t + c_2\,\mathrm{Feb}_t + \ldots + c_{11}\mathrm{Nov}_t + \varepsilon_t \quad (1)$$

In this model, a is the intercept, b_t represents the linear trend over time, and c_1 to c_{11} capture the monthly seasonal effects, with December serving as the reference month. The residual term ε_t accounts for unexplained variability.

We applied this analysis in two spatial formats: (a) coastal areas, averaging from the coastline up to 1° offshore using a 1° latitudinal resolution and (b) the whole area SST grid, where the analysis is made at each grid point.

Furthermore, linear trends in SST over time for the entire period (Table S1 in Supporting Information S1) were computed for two different periods based on AMO patterns: 1982–2020 and 1998–2020.

2.3.4. Monthly Trends

To evaluate seasonal changes, including upwelling duration, monthly trends were assessed by applying linear regression models to the time series of each calendar month (e.g., all January months), using year as the independent variable. As before, these analyses were carried out at each 1° latitude.

2.3.5. Teleconnections

The following climatic indices at monthly resolution were used in this study:

1. The Atlantic Multi-decadal Oscillation Index (AMO; Enfield et al., 2001) was calculated from the SST data of Kaplan et al. (1998) as the de-trended area-weighted average over the North Atlantic (0°−70°N).
2. The NAO climate index was retrieved from NOAA's Climate Prediction Center (https://www.cpc.ncep.noaa.gov/data/teledoc/telecontents.shtml) at monthly temporal resolution. NOAA calculates this index as the rotated PCA (principal component analysis) of monthly means of the 500-mb geopotential height anomaly over the northern hemisphere.

In order to evaluate the effect of these climatic indices, a Pearson's correlation test was applied to the time series data set.

2.3.6. High Spatial Resolution and Isotherm Displacement Analysis

High spatial resolution data were used to decrease bias in the trends derived from the spatial scale. On this monthly high resolution SST data set (Table S1 in Supporting Information S1) we carried out the following analyses:

1. A trend assessment (as described in Section 2.3.3) was applied to each pixel time series.
2. Following the approach of Benazzouz et al. (2014), a coastal upwelling index was calculated using SST data. The SST-based index, UI^{SST}, is defined as the difference between the ocean SST (SST_{ocean}) and the coastal SST (SST_{coast}) at each latitude:

$$UI^{SST} = SST_{ocean} - SST_{coast} \quad (2)$$

   Here, SST_{ocean} refers to the sea surface temperature at longitude 44.975°W, approx. 2,900 km from the nearest point on the coast, which is sufficiently offshore to avoid the effects of upwelling.
3. The velocity of isotherm displacements was calculated on three fixed longitudes (20.025, 24.025 and 28.025°W) by applying Equation 1 considering the latitude position of the isotherms in each year.

3. Results

3.1. Delineation

3.1.1. Climatologies

Climatologies provide a static picture of the system. Four main areas can be observed based on the seasonal climatologies that cover the entire latitudinal extent of the southern CCLME (i.e. 24 time series, Figure 3).

A southern area, stretching from Guinea-Bissau to Cape Blanc in the North of Mauritania (12–21°N), which is characterized by a strong seasonal component. UI^{W} peaks in the southernmost stretch of this area during winter moving to late spring-early summer as we move northwards. Sea Surface Temperature (SST) displays a strong seasonal cycle peaking in late summer-autumn. Chlorophyll maximum values extend from late winter to early summer and abruptly drop in June–July. Dust deposition is variable but on average higher in winter.

A southern-middle area, from Western Sahara to Morocco (22°–26°N), which presents a permanent upwelling (positive UI^{W}) and comparatively constant SST (Figures 3a and 3b). Chlorophyll levels reach higher values later in the year, during summer-autumn. Dust levels are still important but lower compared to the previous area (Figures 3c and 3d).

A northern-middle area from south Morocco (27°–29°N), which experiences a weaker summer upwelling (positive UI^W) and relatively much lower chlorophyll and dust values compared to the southern-middle area (Figure 3).

A northern area (30°–35°N), which presents a spring-summer upwelling UI^W and very low levels of chlorophyll and dust concentrations compared to all other areas (Figure 3).

Similar patterns are observed in the UI^W calculated using the ERA5 database, although with lower intensity values (Figure S1 in Supporting Information S1). Some differences in the intensity patterns are also noted: the highest intensity is observed in the southern area in the NOAA data set (Figure 3), whereas in the ERA5 data set, the highest UI^W is observed in the intermediate region (Figure S1 in Supporting Information S1). Nevertheless, the seasonal patterns remain consistent across both data sets.

3.1.2. Wavelet Analysis

The cluster analysis carried out on the 24 local Wavelet Power Spectrum (WPS) revealed four subregions (i.e., four clusters Figure 4a). The WPSs of the time series for each latitude are available in supplementary material (Figure S2 in Supporting Information S1) and one WPS for each identified subregion is presented in Figure 4b.

The results for the overlapping period (1998–2020) delimit four similar areas (Figure S3 in Supporting Information S1). Similar results were also obtained using the ERA5 data set.

The cluster A (12–17°N, Guinea-Bissau-Cape Blanc area) encompasses the time series from the southernmost latitudes. Here, the annual component accounts for most of the variability and although it is present and significant throughout the series, its amplitude varies in time. Notably, it weakened in several periods (1982–1983, 1989–1990, 1996–1997 and 2004–2005) (Figure 4 and Figure S2 in Supporting Information S1).

The cluster that is the most similar to cluster A is cluster D (29–35°N) that contains the time series from the northernmost latitudes. Similarly, to cluster A, its main mode of variability is annual. The local WPS revealed that this annual component was especially strong from 1998 to 2003 (Figure 4 and Figure S2 in Supporting Information S1).

Indeed, time series from cluster B (18–24°N, Western Sahara) presented a continuous and significant annual component, but other components, such as a 3-year component, accounted for an important part of the total variability. In all the series of this cluster, the amplitude of the annual component was higher at the beginning of the series and during the second half of the series. From 1980 to 1995, the annual component weakened. It is worth noting that during this period there was also less variability in high frequencies (i.e., periods shorter than 6 months) with almost no significant areas in the WPS (Figure 4 and Figure S2 in Supporting Information S1).

Time series in cluster C (26 and 28°N, South Morocco) also displayed the annual component as its main mode of variability. Low-frequency components with periods longer than 5 years are also shown and account for an important share of the variability (Figure 4 and Figure S2 in Supporting Information S1).

3.2. Trends

The analysis reveals four latitudinally coherent subregions, each exhibiting distinct behaviors across the study domain (Figure 5). These differences are reflected in the spatial patterns of upwelling, sea surface temperature, chlorophyll concentration, and dust deposition.

Different UI^W trends are observed along the latitudinal gradient for the longest time series (1967–2020) (Figure 5a). In the southernmost part of the domain (12–18°N, Guinea-Bissau to Cape Blanc, Mauritania), upwelling shows a weakening tendency, which is accompanied by a significant warming between 1982 and 2020 (Figure 5b). This area exhibits the strongest warming across the study region and matches with a marked decrease in chlorophyll concentration from 1998 to 2020 (Figure 5c). Dust deposition also shows a significant decline from 1980 to 2020 (Figure 5d). When restricting the analysis to the overlapping period (1998–2020), upwelling increases except off Guinea-Bissau (12–14°N), the warming trend is no longer detected (Figure 5e), and the dust decrease disappears (Figure 5h).

Between 18 and 25°N, upwelling intensifies significantly over the longest period (1967–2020) (Figure 5a). Despite this strengthening, a warming trend is still detected from 1982 to 2020 (Figure 5b), although it remains

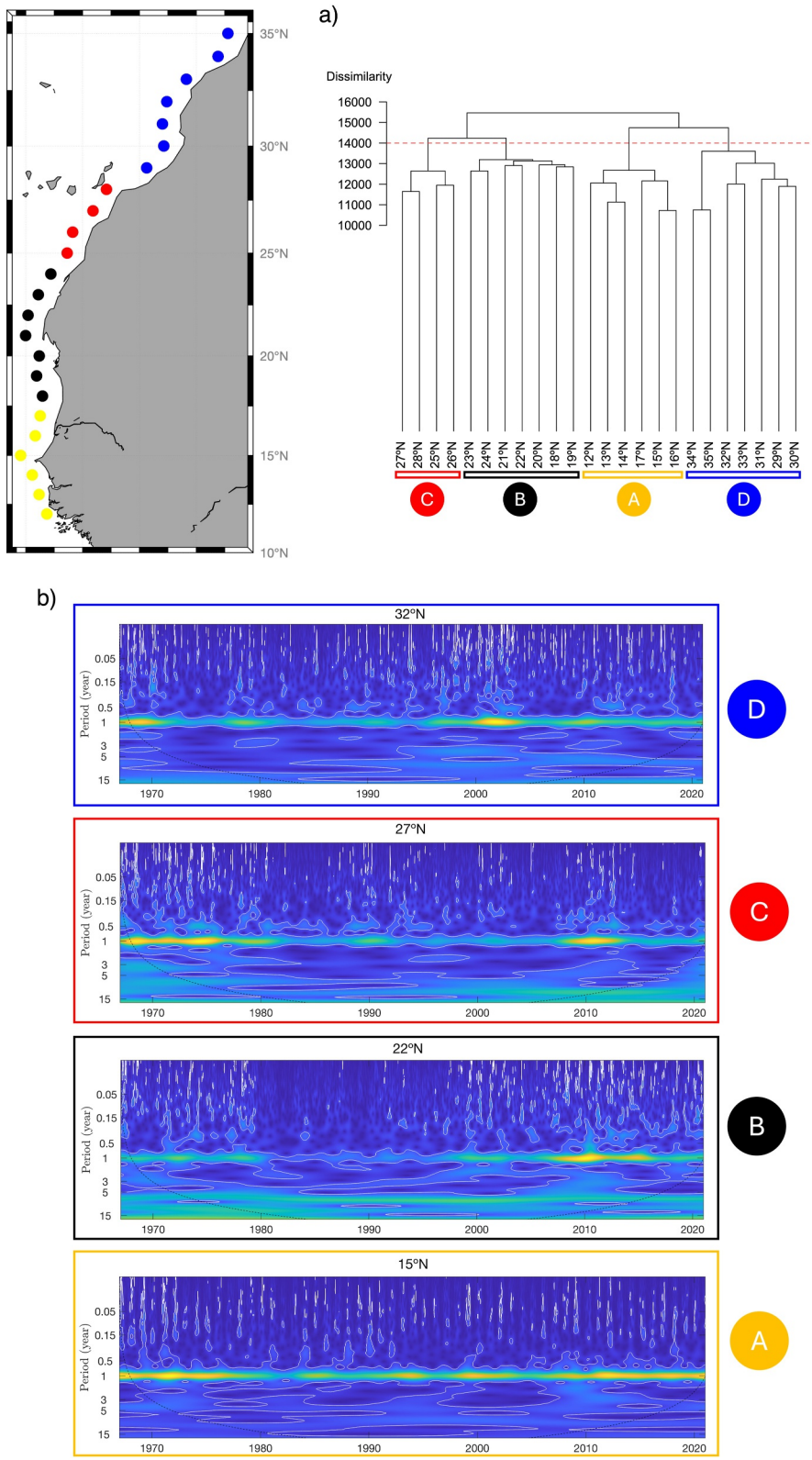

Figure 4.

weaker than in the southern latitudes. Chlorophyll shows a decreasing tendency over 1998–2020 (Figure 5c). Dust deposition in this latitudinal band exhibits a significant decrease from 1980 to 2020, a trend that remains detectable when restricting the analysis to the overlapping period (1998–2020) (Figures 5d and 5h). During this overlapping period, upwelling displays trends consistent with those observed over the longest time series; however, no significant cooling or warming trend is detected.

Further north, between 26°N and 28°N, upwelling weakens over the 1967–2020 period (Figure 5a) in contrast with the neighboring latitudinal bands. This area also experiences warming between 1982 and 2020 (Figure 5b), together with a decrease in chlorophyll from 1998 to 2020 (Figure 5c). Dust deposition shows a significant decline over 1980–2020 (Figure 5d). However, for the overlapping period (1998–2020), upwelling trends become positive and the warming signal disappears (Figure 5e).

In the northernmost part of the study area (29–35°N), upwelling intensifies significantly over the longest time series (1967–2020) (Figure 5a). A warming trend is detected from 1982 to 2020 (Figure 5b), while chlorophyll trends from 1998 to 2020 are weak and slightly positive only at the northern edge (34–35°N) (Figure 5c). In contrast to southern latitudes, dust deposition increases significantly from 1980 to 2020 (Figure 5d). This increasing dust trend is no longer evident when the analysis is restricted to the overlapping period (1998–2020), during which upwelling strengthens and no significant warming is detected (Figures 5e and 5h).

When analyzing UI^W patterns from the ERA5 database, slight differences emerge, with the southern area extending northward to approximately 21°N (Figure S4 in Supporting Information S1). In addition, the weakening trend in UI^W observed in southern Morocco is not reproduced in the ERA5 data for either time period (Figure S4 in Supporting Information S1).

3.2.1. Monthly Trends

The monthly trends analysis reveals the same four latitudinally coherent bands identified in the annual trends, each showing distinct seasonal dynamics along the study domain (Figure 6).

Bakun's upwelling trends by months (1967–2020) varied markedly across latitudes. A general intensification is observed from January to August in the area off North Morocco (29–35°N). In contrast, the area off South Morocco (25–28°N) showed a marked decrease in summer-autumn. The seasonal pattern changes again in the Western Sahara area (19–24°N), which shows an increase in spring-summer (Figure 6a), resembling that of North Morocco. These contrasting neighboring trends are responsible for the subdivision of this region. The southernmost region showed weaker negative trends.

Monthly sea surface temperature trends (1982–2020) displayed a homogeneous pattern across the latitudinal gradient, indicating an overall warming. However, positive trends were more evident in the southernmost area from June to December (Figure 6b). Interestingly, the upwelling decrease detected in the area off south Morocco did not result in a marked warming in this region.

Scattered negative monthly chlorophyll trends were observed across the whole latitudinal gradient from 1998 to 2020, particularly during the central months of the year (Figure 6c).

Dust trends from 1980 to 2020 did not exhibit a clear pattern except for a decrease during the winter months in the southernmost stretches of the area (Figure 6d), which could partly explain the chlorophyll decrease in this area together with the UI^W decrease.

Most of the previously reported trends weakened when restricting the analyses to the overlapping decades (1998–2020) (Figure 6). The upwelling intensification trends off Western Sahara and North Morocco are now restricted to summer and winter, respectively. Similarly, the weakening trends of the Guinea-Bissau–Cape Blanc area are now limited to summer and autumn. Most of the sea surface temperature trends also disappeared,

Figure 4. Comparison of the local Wavelet Power Spectrums (WPS) computed on the time-series of upwelling index from NOAA for each degree of latitude (12°N to 35°N). Panel (a) hierarchical cluster, based on Ward (1963). Each WPS represents a branch of the dendrogram and is indicated by its latitude. The shorter the distance between the different WPS, the more similar they are. The discontinuous red line indicates the dissimilarity threshold used. Panel (b) selection of four WPSs, indicative of the clusters A, B, C and D, respectively. In each WPS, the power values are color-coded on a spectrum ranging from blue (indicating low values) to orange (representing high values). The dark dashed line delineates the cone of impact, below which the information is influenced by edge effects. White contours designate the 5% significant areas determinate with a bootstrapping scheme.

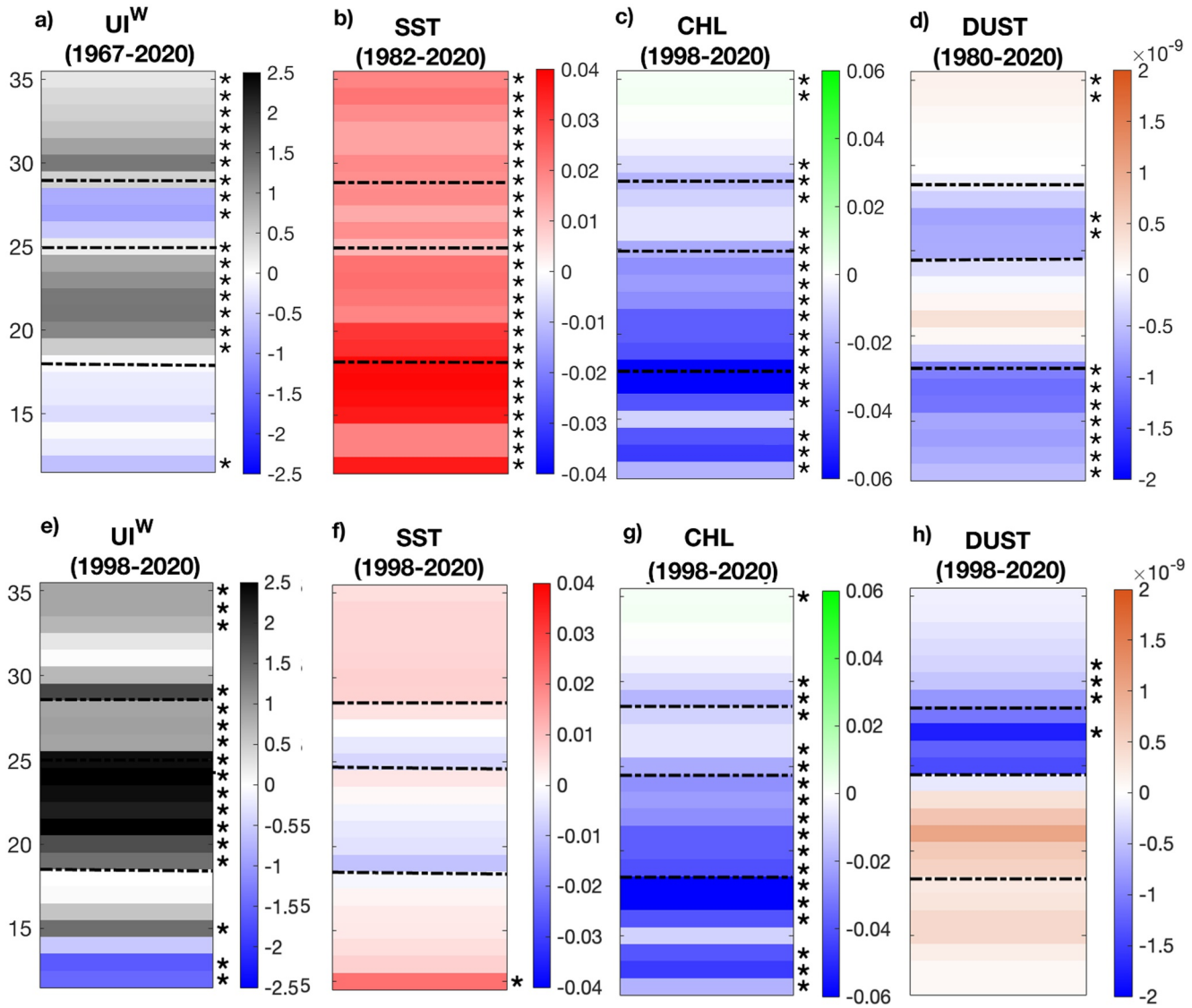

Figure 5. Annual trends. Trends of the Bakun upwelling index (UI^W; $m^3\ s^{-1}\ 100\ m^{-1}\ yr^{-1}$), sea-surface temperature (SST; $°C\ yr^{-1}$), chlorophyll-a (CHL; $mg\ m^{-3}\ yr^{-1}$), and dust deposition ($kg\ m^{-3}\ yr^{-1}$) at each latitude are shown for the longest available time series (a–d) and for the overlapping period 1998–2020 (e–h). An asterisk (*) marks when trends (values in colored legend) are significant (p-value <0.05). Dashed lines separate the different subregions.

remaining only some of them between July and November in the south and between November and December in North Morocco. In terms of dust input, a negative trend in summer to spring off Western Sahara-North Morocco and a positive trend from June to July and from September to October in the south are registered.

As observed in the annual trends (Figure S4 in Supporting Information S1), the decrease in upwelling in the southern Morocco region during the 1967–2020 period is not as evident when using ERA data. However, this trend is observed during the 1998–2020 period, in contrast to what is seen in NOAA data (Figure S5 in Supporting Information S1).

3.2.2. High Spatial Resolution and Isotherm Displacement Analysis

The thermal upwelling index reveals the same trends observed when using the Bakun's index, with an increase in the intensity in the Western Sahara and North Morocco areas (Figures 5 and 7 and Figure S6 in Supporting Information S1). These trends seem to be responsible for a decrease in coastal sea surface temperatures, which contrasts with the warming trend observed in the southern area, where the thermal upwelling index also shows a

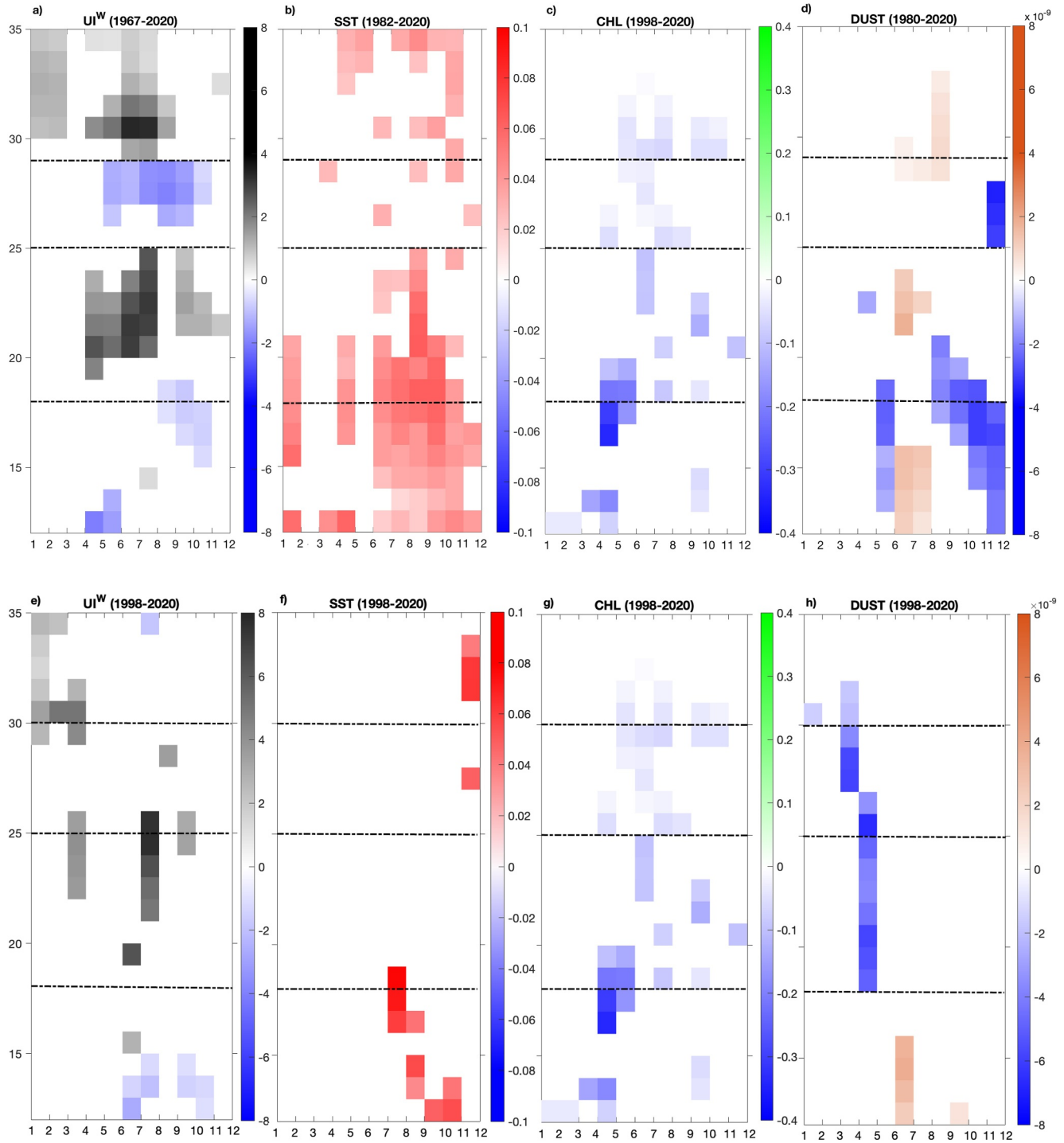

Figure 6. Monthly trends. Monthly trends of the Bakun upwelling index (UI^W; $m^3\ s^{-1}\ 100\ m^{-1}\ yr^{-1}$), sea-surface temperature (SST; $°C\ yr^{-1}$), chlorophyll-a (CHL; $mg\ m^{-3}\ yr^{-1}$), and dust deposition ($kg\ m^{-3}\ yr^{-1}$) at each latitude are shown for the longest available time series (a–d) and for the overlapping period 1998–2020 (e–h). Colors indicate trend magnitude and direction, with only statistically significant trends shown; white areas denote non-significant trends ($p > 0.05$), and dashed lines separate subregions.

weakening, and so does in the offshore areas (Figure S6 in Supporting Information S1). As observed in the trend analysis (Figures 5 and 6), these patterns are more pronounced when analyzing data from 1996 to 2021 than from 1982 to 2020, where the decrease sea surface temperature trend is only observed in the main upwelling areas (Cape Ghir, Cape Juby, Dakhla, Cape Blanc) (Figure 7). The analysis also reveals monthly variations,

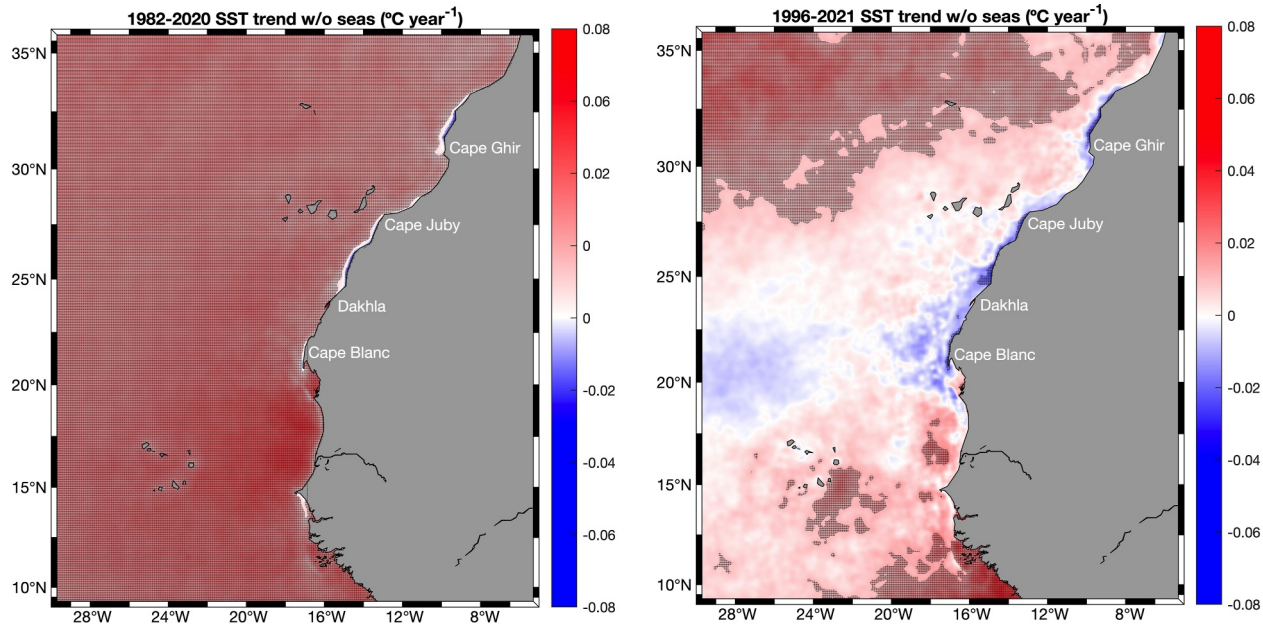

Figure 7. Raster trends. Decadal sea surface temperature (SST) linear trends for the period of 1982–2020 (left) and 1998–2021 (right). The black dots represent points with significant trends (p-value <0.05).

highlighting a cooling trend on the north coast from spring to autumn. Significant cooling trends are observed in the summer during both time periods, particularly in the main upwelling areas, consistent with the upwelling index variations shown in Figure 6. Significant variations are also observed in the winter in the northern Morocco in the UI^{SST}, but not in the sea surface temperature trend analysis. Additionally, a pronounced warming trend is evident on the south coast in all periods and analyses.

A significant displacement of the 18, 19, 20, and 21°C isotherms toward higher latitudes is observed, with the greatest velocities occurring the further from the coast (Figure S7 in Supporting Information S1).

3.3. Teleconnections

To assess whether the observed trends are linked to the AMO and/or the NAO, we conducted a correlation analysis between these climate indices and the variables.

The AMO showed the strongest significant correlations ranging from −0.62 to 0.81. Negative correlations were observed between this index and upwelling, chlorophyll and dust deposition in the southern area from Guinea-Bissau to Cape Blanc. Off South Morocco, negative correlations were also observed between the AMO and upwelling and chlorophyll but not with dust. Conversely, positive correlations were observed between the AMO and upwelling and dust off northern Morocco. It is also worth stating the significant and high positive correlation between sea surface temperatures and the AMO across all latitudes (Figure 8).

The NAO exhibited opposite correlations with the variables compared to the AMO, with a positive correlation with upwelling, which negatively correlated with sea surface temperature and a positive correlation with chlorophyll. Correlations with dust presented different patterns, being positive in the south and negative off North Morocco (Figure 8).

4. Discussion

4.1. Subregionalization of the Southern CCLME

The primary objective of the study was to identify coherent subregions across the latitudinal extent of the southern CCLME based on their physical and biogeochemical features while also capturing historical long-term trends. Using a combination of environmental variables and time-series analyses (seasonal regression models and

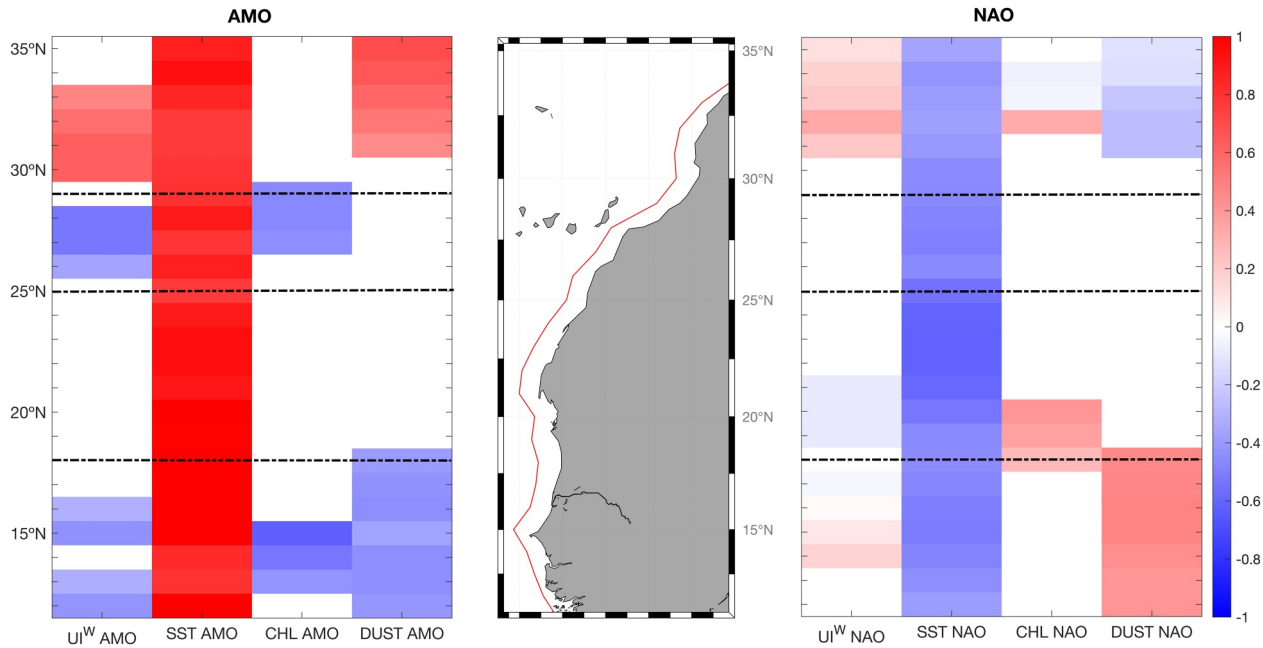

Figure 8. Teleconnections. Significant correlations (Pearson's correlation, p-value <0.05) for each coastal series (longest period of each variable) with the AMO (left panel) and NAO (right panel) indices. Dashed lines separate the different subregions. Upwelling index was calculated from NOAA (Table S1 in Supporting Information S1).

wavelets), we delineated four distinct subregions (Figure 9). The four subregions display distinct seasonal cycles and long-term tendencies:

1. The tropical subregion (12°–18–21°N) presents a winter-spring upwelling, a strong seasonal cycle of SST, a highly variable dust deposition (peaking in winter) and an elevated chlorophyll concentration in winter and spring, which drops abruptly in summer. This region presents a coherent weakening of upwelling and a warming trend across the whole area (Figure 5). The clearest negative chlorophyll trend is also detected in this subregion along with significant dust reduction during the long-term period analysis (Figure 5) that disappeared in recent times (Figure 5). This subregion exhibits a marked upwelling seasonality with a decreasing trend from spring to autumn (Figure 6), which produces an overall reduction in the duration of the upwelling (Figure S8 in Supporting Information S1).
2. The Western Sahara subregion (19–22–25°N) exhibits increasing wind-driven upwelling and decreasing sea surface temperature and chlorophyll trends (Figure 5).
3. The South Morocco subregion (26–28°N) shows a similar pattern to the Western Sahara subregion with increasing upwelling and decreasing sea surface temperature and chlorophyll trends (Figure 5). However, unlike the Western Sahara subregion, which maintained an increasing upwelling trend, the South Morocco subregion experienced a significant decrease in upwelling in some trend analysis (Figures 5a and 6a and Figure S5b in Supporting Information S1).
4. The North Morocco subregion (29–35°N) is characterized by a weak summer upwelling and lower sea surface temperatures and dust and chlorophyll values in comparison with the rest of the subregions. Here, the upwelling intensification is not able to counteract the overall warming trend except in Cape Ghir (Figure 7 and Figure S6 in Supporting Information S1). An increasing trend in chlorophyll levels as well as in dust concentration was observed in this subregion (Figures 5c and 5d). However, the dust long-term trend changes from positive to negative in the overlapping time period (Figure 5h).

While there are no significant variations in the annual component of wavelets detected in the North Morocco subregion (Figure S2 in Supporting Information S1), these results appear to arise from a combination of intensified upwelling during spring and winter (Figure 6) and an extended duration of the upwelling season in recent years, particularly during the winter months (Figure S8 in Supporting Information S1). Nonetheless, no

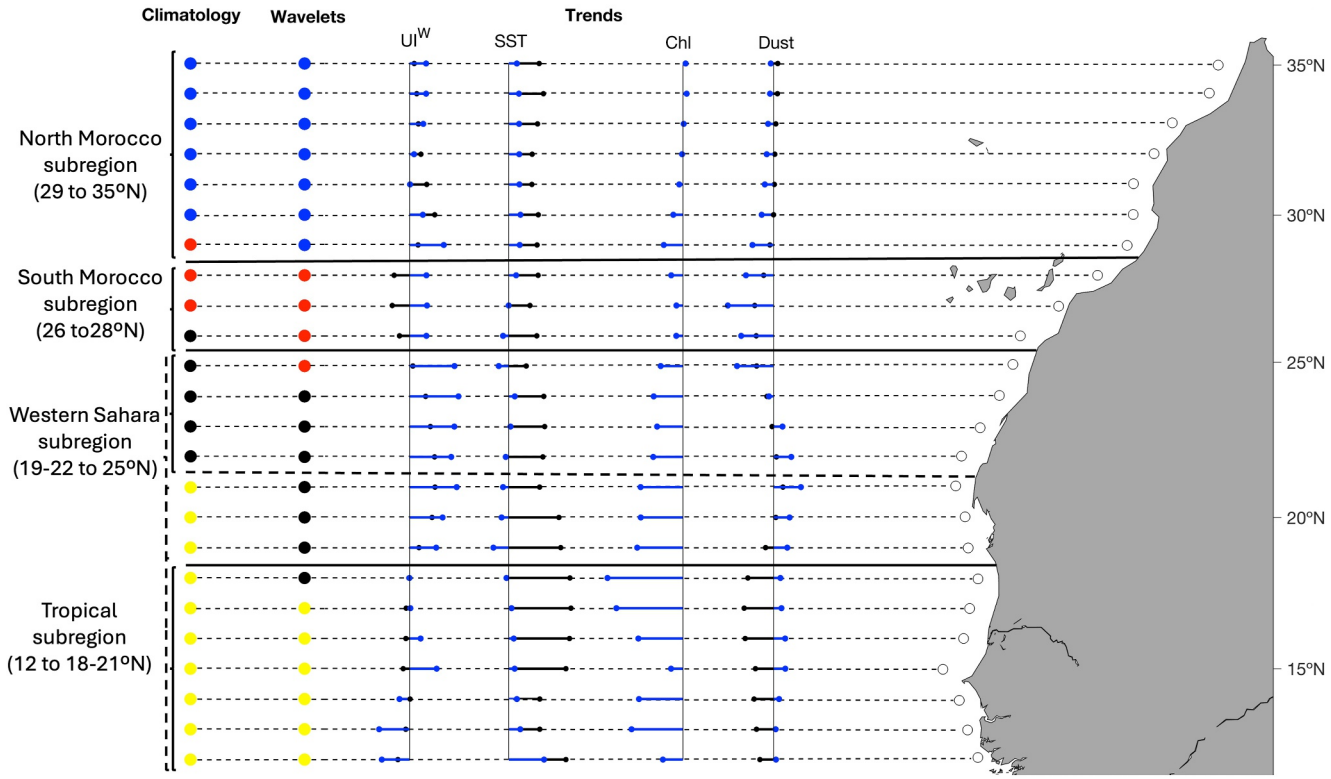

Figure 9. Overview of results. From left to right. The first color-coded line of points represents the different subregions based on the climatologies. The second color-coded line shows subregions based on Bakun's upwelling index (UI^W, 1967–2020) wavelet results. The next four panels show trends, the length of the arrow is proportional to the trend value and the direction refers to the sign (positive to the right). Black lines represent the longest available period for each variable -UI^W (1978–2020), sea surface temperature (SST, 1982–2020), chlorophyll-a (CHL, 1998–2020), and Dust (1980–2020)- while blue lines indicate the overlapping period (1998–2020), with values plotted at each latitude.

significant chlorophyll monthly trends were observed except for decreasing trends in the northern part (Figure 6), primarily occurring during the central months of the year.

These robust findings align with previous classifications (e.g., Arístegui et al., 2009; Cropper et al., 2014) sharing a single coherent subregion between 12° and 18–21°N (i.e., the tropical subregion). It is worth noting that the delimitation of this subregion differs slightly from one time series analyze to another. For example, the northern limit of the tropical subregion is identified at 17°N in the wavelet analysis and at 18°N in the annual and monthly analyses, but further north, at 21°N in climatologies.

Climatologies are the only method used in this study that does not incorporate long-term trends, which suggests that the trends south of 17–18°N differ from those observed between 18 and 21°N. This distinction aligns, to some extent, with the findings of Sylla et al. (2019) and Vázquez et al. (2023), who describe weaker upwelling between 12 and 15°N and stronger upwelling with more pronounced seasonality between 16 and 20°N.

The remaining subregions (i.e., Western Sahara subregion, Southern Morocco subregion and Northern Morocco subregion) are largely consistent with the subdivision proposed by Cropper et al. (2014), which is based on the seasonality and intensity of upwelling. However, we identify two distinct subregions within the area previously defined as a Weak Permanent Annual Upwelling Zone (26–35°N), in agreement with the findings of Vázquez et al. (2022), who reported a similar subdivision based on ROMS simulations.

4.2. Mechanisms Driving Trends in Oceanographic Variables

4.2.1. Sea Surface Temperature Trends and Their Relation to Upwelling

A clear discrepancy emerges regarding which regions exhibit sea-surface warming and which do not, a pattern that appears to be influenced by the spatial resolution used in the analyses. Low-resolution analyses may not fully

capture the underlying response, as averaging over larger areas can obscure localized cooling signals by blending them with adjacent warming regions. This effect, where different resolutions yield different responses, has been previously documented (Sylla et al., 2022).

In contrast, our high-resolution analysis reveals a significant SST decrease along the coastal zones of the North Morocco, the South Morocco, and the Western Sahara subregions (Figure 7), associated with an intensification of the wind-driven UI in these areas (Figure 5 and Figure S6 in Supporting Information S1). This buffer effect was previously reported by Varela et al., 2018, who found that 92% of the coastal upwelling regions displayed a mitigated trend compared to offshore. Varela et al. (2022) similarly projected this response under an SSP5-8.5 scenario, identifying a pronounced offshore warming trend and a comparatively weaker warming signal in coastal areas, which contrasts with the clear decreasing sea surface temperature trend detected in this study. This discrepancy may be attributed to the lower resolution used in the studies by Varela et al. (2018, 2022) compared to the resolution employed here. This marked decrease in sea-surface temperature, associated with an intensification of the UI, is also supported by evidence from a 2,500-year sediment-core record near Cape Ghir (McGregor et al., 2007).

Other authors observed a warming trend throughout the entire CCLME region (Barton et al., 2013; Gómez-Letona et al., 2017; Kessler et al., 2022; Marcello et al., 2011). This result, detailed further in Section 4.2.5, may be associated with the effects of the Atlantic Multidecadal Oscillation (AMO) in this region. Specifically, analyses based on time series extending prior to 1996 indicate a warming trend across the whole region, corresponding to a shift in the AMO phase from negative to positive. However, this warming trend disappears in coastal areas when the analysis is limited to the period after 1996, coinciding with a positive phase of the AMO.

4.2.2. Variability, Intensification, and Duration of Upwelling

Based on the observed upwelling trends, a noticeable differentiation emerges between the northernmost and southernmost zones. In the southern zone (the tropical subregion), there is a distinctive seasonal upwelling pattern, which shows a decreasing trend in duration. In contrast, the North Morocco subregion exhibits an extension in both duration and intensity, rendering it permanent and resembling the permanent upwelling of Western Sahara (Figure S8 in Supporting Information S1).

The Western Sahara subregion shows an increase in the annual component of the upwelling, while the duration remains constant and persists year-round (Figures S8 and S9 in Supporting Information S1). However, the intensity of upwelling is increasing, mainly during spring and summer (Figure 6). Variations in the intensity and duration of the upwelling are also predicted by Wang et al. (2015). These authors identified an increase in upwelling intensity and an extension of the upwelling season by several days per decade from 1950 to 2099 at higher latitudes, corresponding to the observed trend in the North Morocco subregion (Figure 5 and Figure S8 in Supporting Information S1). However, they found a decrease in upwelling intensity at lower latitudes, with no variation in its duration. In our case, we also noted this weakening trend but was associated with a decrease in duration (Figure S8 in Supporting Information S1).

The South Morocco subregion, shows a transition from permanent to seasonal upwelling features over the years (Figure S9 in Supporting Information S1). This subregion presents high annual variability showing a stronger similarity with either the Western Sahara or the North Morocco subregions depending on the year. Consequently, it remains uncertain whether this area will tend to homogenize with the neighboring Western Sahara to the south, the North Morocco to the north or to further differentiate from them. This variability may explain the differing signals across data sets and time periods.

The increase in the upwelling intensity in the Western Sahara subregion could be the reason for the decreasing trend observed in offshore SST in this subregion (Figure 7), in contrast to the rest of the subregions. Another possible explanation for these variations relates to the influence of atmospheric dust, which has been proposed as a driver of temperature anomalies along the West African coast (Chen et al., 2021). They observed a cooling trend at 22°N and 11°N, extending to 30°W and 55°W, as well as a warming trend between 0–20°N and 25–35°N. These findings could help interpret the patterns observed in this study.

4.2.3. Biological Response: Divergent Chlorophyll-a Trends

The overall decreasing trends observed in chlorophyll-a are consistent with previous findings based on MODIS observations (Arístegui et al., 2009; Gómez-Letona et al., 2017). However, the increase in upwelling intensity in the Western Sahara subregion does not correspond to a rise in chlorophyll, which instead exhibits a decreasing trend. Changes in dust input may contribute to this behavior, but the relationship remains uncertain, as both increasing and decreasing trends are observed across the periods analyzed. Another possible explanation for this discrepancy could be a change in local stratification, with implications in the mixed-layer depth and the depth from which upwelling waters are drawn. Stronger stratification can lead to shallower source depths and reduced nutrient supply (Jacox & Edwards, 2011; Lentz & Chapman, 2004). This could explain the apparent discrepancy between upwelling and chlorophyll trends. Furthermore, these variations could be attributed to a reduction in the surface area of upwelling origin due to a less active westward propagation, attributed to the overall weakening of the Northeast Trade Winds in the inner region of the tropical Atlantic water area (Polonsky & Serebrennikov, 2018).

Other possible explanations include changes in the biogeochemical properties of upwelled water masses driven by processes operating beyond the spatial and temporal scales of the EBUS, such as water-mass formation and ventilation under long-term climate change (Pitcher et al., 2021; Rykaczewski & Dunne, 2010). Variations in basin-scale ocean–atmosphere modes and their teleconnections (e.g., ENSO) (Bonino et al., 2019) can affect winds (Jacox et al., 2015), circulation (Montes et al., 2011), eddy behavior (Conejero et al., 2020), water-mass composition (Bograd et al., 2019), and biogeochemical characteristics (Garçon et al., 2019), thereby influencing EBUS source waters and coastal inputs (Dunn et al., 2018). Further analyses are needed to identify the dominant drivers of these signals.

4.2.4. Large-Scale Atmospheric and Oceanic Forcing Mechanisms

Our results suggest a northward shift of the upwelling regions, supported by previous studies (Seabra et al., 2019; Varela et al., 2022). This northward shift is expected to lead to temperature homogenization driven by a weakening of upwelling in the southernmost areas. In contrast, the temperature difference between the coast and ocean is expected to increase due to the strengthening of upwelling in the northern part of the region. Several studies (Rykaczewski et al., 2015; Sousa et al., 2017a; Sylla et al., 2019; Varela et al., 2022) hypothesized a poleward displacement of the Azores High, which could potentially explain these observed patterns. Another possible explanation concerns the intensification and northward displacement of the Intertropical Convergence Zone (ITCZ), which could also account for the observed temperature increase in the tropical subregion (12–21°N) (Bryne et al., 2018). The ITCZ marks the convergence of trade winds from both hemispheres, and its northward shift can weaken the trade winds in the lower latitudes of the Northern Hemisphere. This weakening reduces the intensity of upwelling in the southern sCCLME, limiting the supply of cold, nutrient-rich waters and favoring surface warming.

4.2.5. Large-Scale Climate Modes

Some of the variability of the oceanographic and biogeochemical variables is expected to be associated to large scale climate patterns, such as the Atlantic Multidecadal Oscillation (AMO) and the North Atlantic Oscillation (NAO) (Marrero-Betancort et al., 2020; Narayan et al., 2010; Pardo et al., 2011).

In general, it is widely accepted that during the negative phases of the AMO in the North Atlantic, an amplification of the subtropical high-pressure system results in increased winds favorable for upwelling around the Canary Islands (Alexander et al., 2014; Marrero-Betancort et al., 2020; Pardo et al., 2011). This relationship implies a negative correlation between upwelling-favorable winds and the AMO index. These findings are aligned with our results, which showed a positive correlation between the AMO and sea surface temperatures across the entire sCCLME (Figure 8). We also noted a significant negative correlation between the AMO and upwelling and chlorophyll in the tropical and South Morocco subregions. Interestingly, a positive correlation with upwelling was observed in the North Morocco subregion (Figure 8). It is important to be cautious when interpreting these correlations since the primary time cycle of the AMO spans roughly 70 years.

The increasing intensity of the winds also appears to affect the dust deposition in the area with a negative correlation of the AMO with dust in the tropical subregion, in contrast with a positive correlation in the South Morocco subregion (Figure 8).

The signal of the AMO in the region could account for the contrasting trends observed between the overlapping and longer periods. A transition from a negative phase of the AMO to a positive phase occurred in 1995, which may explain the shift from a positive sea surface temperature trend between 1982 and 2020 to a trend that was no longer significant from 1998 to 2020 (Figure S10 in Supporting Information S1).

However, the use of the AMO as an explanatory framework remains a matter of active debate. Recent studies have questioned not only its physical interpretation but also its statistical validity as an internally generated mode of climate variability (e.g., Mann et al., 2021), arguing that what is commonly identified as the AMO may instead reflect the imprint of external forcings or methodological artifacts associated with detrending procedures. In this context, the apparent correspondence between SST trends and AMO phase changes should be interpreted with caution. Rather than implying a direct causal relationship, the AMO is considered here as a descriptive index capturing low-frequency Atlantic variability that may co-occur with the observed trends. Consequently, the differences between the long and overlapping periods may arise from a combination of phase-dependent variability, limited temporal coverage, and the influence of external forcings, rather than from a single dominant climate mode.

The NAO also exerts an influence on the region, although weaker than AMO (Figure 8). A positive phase of the NAO typically leads to a reinforcement of the Azores High and the Iceland Low, resulting in stronger winds that intensify upwelling processes (Georg et al., 2022). Our findings appear to align with these results, revealing a significant correlation with upwelling, particularly in the tropical and North Morocco subregions (Figure 8). This correlation corresponds to a decrease in sea surface temperature (a pattern observed throughout the entire sCCLME) and an increase in chlorophyll concentrations.

The NAO influences not only the intensity of NW African coastal upwelling but also the supply of Saharan dust into the eastern North Atlantic, where winter observations show high variability in African dust export over southern Mauritania and the tropical Atlantic (mainly north of 15°N) (Chiapello et al., 2005).These results support our findings of a positive trend observed in the tropical subregion that correlates with the NAO (Figure 8). However, we also observed a negative correlation in the South Morocco subregion, which may indicate a different control of the transport of the wind in this area (Figure 8).

Although the AMO and NAO appear to have an influence in the area, their impacts do not seem to be the sole cause of the trends described in the present study.

4.3. Implications for Projections and Ecosystem Management

Recent studies indicate that climate change impacts in the southern Canary Current Large Marine Ecosystem (sCCLME) are spatially heterogeneous. While our results show a coherent present-day pattern in the whole tropical region, projections under high-emission scenarios (RCP8.5) suggest locally differentiated responses in winds, stratification, and upwelling source-water depth (Sylla et al., 2019; Vázquez et al., 2023). In the broader sCCLME, some studies project intensified wind stress curl and geostrophic upwelling leading to deeper source waters, particularly off South Morocco (Chang et al., 2023; Jing et al., 2023), whereas others report increased stratification and contrasting north–south trends in upwelling depth within the tropical subregion (Vázquez et al., 2023, 2024). Additionally, projected offshore warming under RCP8.5 (Varela et al., 2022) contrasts with the cooling trend observed in this study, underscoring the complexity and uncertainty of future sCCLME responses.

In this context, the subregional differentiation identified here provides a useful observational framework for interpreting and validating the heterogeneous responses simulated by Earth System Models. Rather than contradicting previous studies, our results suggest that the often contrasting projections under high-emission scenarios reflect the spatial complexity of the sCCLME. The recent regional responses, characterized by weakened and shortened upwelling in the tropical subregion, intensified and more persistent upwelling in northern areas, and transitional behavior of South Morocco, closely mirror the range of future responses projected for winds, stratification, and source-water depth. From a management perspective, these findings reinforce the limitations of defining management units based solely on geopolitical boundaries (van Hoof, 2015) and emphasize the

importance of identifying bio-hydrographically coherent regions as a foundation for ecosystem-based management (Bindoff et al., 2019), thereby improving the resilience and sustainability of sCCLME marine ecosystems under ongoing environmental change.

4.4. Limitations of the Study

In this study, the upwelling index is calculated using an intermediate resolution database (the NOAA database, Table S1 in Supporting Information S1). Data resolution is known to influence the magnitude of the upwelling index (Jacox et al., 2018; Sylla et al., 2022). Accordingly, we compared a higher-resolution data set (ERA5) with NOAA data and found, consistent with previous studies, that the NOAA data set yields higher upwelling index values. Therefore, the values reported here should be interpreted with caution. Nevertheless, the spatial patterns of upwelling are consistent between the two data sets despite the differences in resolution.

Additionally, the cross-shore geostrophic flow tends to oppose Ekman transport, leading to higher estimates of upwelling when only Ekman transport is considered. To address this issue, another upwelling index, called the Coastal Upwelling Transport Index (CUTI), has been proposed, which takes this issue into account (Jacox et al., 2018). Nevertheless, none of these variations seem to significantly impact the observed trends in the CCLME area (Vázquez et al., 2023, 2024). Hence, the present data set of the upwelling process and derived phenomena collected in this work may be sufficient for the goals of this study.

It should also be noted that the so-called overlapping period (1998–2020, due to short ocean color satellite time series) spans only 23 years, so the results should be interpreted with caution. Furthermore, we acknowledge that the use of fixed coastal bands (1° offshore) may filter subregional filament variability, which could affect fine-scale biogeochemical comparisons.

5. Conclusions

In this work, we have delineated four subregions for the sCCLME, each defined by distinct upwelling dynamics and recent environmental trends.

The tropical subregion (12° to 18–21°N) exhibits strong seasonality, with a decreasing trend in upwelling duration and a coherent warming signal. The fact that its boundaries vary across different analyses further highlights its dynamics and non-stationary nature. This combination of pronounced seasonality, warming, and shifting limits suggests that the tropical subregion may be particularly sensitive and potentially the most vulnerable to climate-driven changes within the southern Canary Current Large Marine Ecosystem.

The Western Sahara subregion (18–21° to 24°N) shows increasing upwelling intensity, yet chlorophyll concentrations are declining, suggesting that upwelling processes alone are not the primary driver of productivity trends.

The North Morocco subregion (25°–28°N) experiences weak summer upwelling, which has become more persistent over time, resembling the Western Sahara subregion.

Similarly, the South Morocco subregion (29°–35°N) mirrors Western Sahara's trends, with intensifying wind-driven upwelling and decreasing sea surface temperature and chlorophyll levels. However, it also exhibits a marked interannual variability, alternating between more seasonal upwelling periods and phases of more persistent upwelling.

These results reveal the complex interactions among upwelling, temperature, and other environmental drivers, providing a high-resolution, observation-based framework to validate the Earth System Model projections. The distinct subregional responses reflect the intrinsic spatial complexity of the southern Canary Current Large Marine Ecosystem and offer a baseline to reconcile seemingly contradictory findings from previous studies.

These insights have potential applications for ecosystem-based management. Defining management areas according to bio-hydrographic characteristics rather than geopolitical boundaries could help tailor management toward more holistic and sustainable resource use, while also contributing to the resilience of marine communities. Additionally, the methodology is broadly applicable to other Eastern Boundary Upwelling Systems, offering a transferable framework that integrates physical, biogeochemical, and atmospheric drivers along with analyses of trends, duration, and seasonality.

Conflict of Interest

The authors declare no conflicts of interest relevant to this study.

Availability Statement

The upwelling index (Bakun Upwelling Index, UI^W) was obtained from two reanalysis products. Daily and monthly upwelling indices at 1° × 1° spatial resolution were obtained from NOAA (https://oceanview.pfeg.noaa.gov/products/upwelling/bakun). Monthly upwelling indices at ~31 km spatial resolution were obtained from the ERA5 reanalysis provided by the Copernicus (https://doi.org/10.24381/cds.f17050d7). Sea surface temperature (SST) data for the period 1982–2021 were obtained from the Copernicus Marine Environment Monitoring Service (CMEMS) (https://doi.org/10.48670/moi-00168). Surface dust concentration data were obtained from the MERRA-2 reanalysis produced by NASA (https://gmao.gsfc.nasa.gov/reanalysis/MERRA-2/). Monthly chlorophyll-a concentration data were obtained from CMEMS (https://doi.org/10.48670/moi-00281). The Atlantic Multidecadal Oscillation (AMO) index and the North Atlantic Oscillation (NAO) index were obtained from the NOAA (https://psl.noaa.gov/data/timeseries/AMO/; https://www.cpc.ncep.noaa.gov/data/teledoc/telecontents.shtml). The software used was R and Rstudio (version 4.0.2) and MATLAB R2020a.

Acknowledgments

This work was supported by the European Union's Horizon 2020 research and innovation programme under Gran Agreement No. 862426 (MISSION ATLANTIC). Extra support from the project in the form of a mobility grant to J. Cabrera-Busto facilitated collaboration with L. Buttay (IMR, Tromsø). This output reflects only the author's view and the Research Executy Agency (REA) cannot be held responsible for any that may be made of the information contained therein. The open acess publication of this articles was funded by Universidad de Malaga/ CBUA.

References

Alexander, M. A., Kilbourne, K. H., & Nye, J. A. (2014). Climate variability during warm and cold phases of the Atlantic multidecadal oscillation (AMO) 1871–2008. *Journal of Marine Systems*, *133*, 14–26. https://doi.org/10.1016/j.jmarsys.2013.07.017

Arístegui, J., Barton, E. D., Álvarez-Salgado, X. A., Santos, A. M. P., Figueiras, F. G., Kifani, S., et al. (2009). Sub-regional ecosystem variability in the Canary current upwelling. *Progress in Oceanography*, *83*(1–4), 33–48. https://doi.org/10.1016/j.pocean.2009.07.031

Bakun, A. (1973). *Coastal upwelling indices, West coast of North America*. US Department of Commerce. NOAA Technical Report, NMFS SSRF-671.

Bakun, A. (1975). Daily and weekly upwelling indices, west coast of North America. *NOAA Technical Report*, *16*.

Barton, E. (1998). Eastern boundary of the North Atlantic: Northwest Africa and Iberia. Coastal segment (18, E). In A. R. Robinson (Ed.), *The Sea* (Vol. 11, pp. 633–657). John Wiley and Sons.

Barton, E. D., Field, D. B., & Roy, C. (2013). Canary current upwelling: More or less? *Progress in Oceanography*, *116*, 167–178. https://doi.org/10.1016/j.pocean.2013.07.007

Baudron, A. R., Brunel, T., Blanchet, M. A., Hidalgo, M., Chust, G., Brown, E. J., et al. (2020). Changing fish distributions challenge the effective management of European fisheries. *Ecography*, *43*(4), 494–505. https://doi.org/10.1111/ecog.04864

Benazzouz, A., Mordane, S., Orbi, A., Chagdali, M., Hilmi, K., Atillah, A., et al. (2014). An improved coastal upwelling index from sea surface temperature using satellite-based approach–the case of the Canary current upwelling system. *Continental Shelf Research*, *81*, 38–54. https://doi.org/10.1016/j.csr.2014.03.012

Bindoff, N. L., Cheung, W. W. L., Kairo, J. G., Arístegui, J., Guinder, V. A., Hallberg, R., et al. (2019). Changing Ocean, marine ecosystems, and dependent communities. In H.-O. Pörtner, D. C. Roberts, V. Masson-Delmotte, P. Zhai, M. Tignor, E. Poloczanska, et al. (Eds.), *IPCC special report on the ocean and cryosphere in a changing climate* (pp. 447–587). Cambridge University Press. https://doi.org/10.1017/9781009157964.007

Bograd, S. J., Jacox, M. G., Hazen, E. L., Lovecchio, E., Montes, I., Pozo Buil, M., et al. (2023). Climate change impacts on eastern boundary upwelling systems. *Annual Review of Marine Science*, *15*(1), 303–328. https://doi.org/10.1146/annurev-marine-032122-021945

Bograd, S. J., Schroeder, I. D., & Jacox, M. G. (2019). A water mass history of the Southern California current system. *Geophysical Research Letters*, *46*(12), 6690–6698. https://doi.org/10.1029/2019GL082685

Bonino, G., Di Lorenzo, E., Masina, S., & Iovino, D. (2019). Interannual to decadal variability within and across the major Eastern Boundary Upwelling Systems. *Scientific Reports*, *9*(1), 19949.

Bretherton, C. S., Smith, C., & Wallace, J. M. (1992). An intercomparison of methods for finding coupled patterns in climate data. *Journal of Climate*, *5*(6), 541–560. https://doi.org/10.1175/1520-0442(1992)005<0541:aiomff>2.0.co;2

Bryne, M. P., Pendergass, A. G., Rapp, A. D., & Wordzicki, K. R. (2018). Response of the intertropical convergence zone to climate change: Location, windth and strength. *Current Climate Change Reports*, *4*, 355–370. https://doi.org/10.1007/s4061-018-0110-5

Cazelles, B., Chavez, M., Berteaux, D., Ménard, F., Vik, J. O., Jenouvrier, S., & Stenseth, N. C. (2008). Wavelet analysis of ecological time series. *Oecologia*, *156*(2), 287–304. https://doi.org/10.1007/s00442-008-0993-2

Cazelles, B., & Stone, L. (2003). Detection of imperfect population synchrony in an uncertain world. *Journal of Animal Ecology*, *72*(6), 953–968. https://doi.org/10.1046/j.1365-2656.2003.00763.x

Chang, P., Xu, G., Kurian, J., Small, R. J., Danabasoglu, G., Yeager, S., et al. (2023). Uncertain future of sustainable fisheries environment in eastern boundary upwelling zones under climate change. *Communications Earth & Environment*, *4*(1), 19. https://doi.org/10.1038/s43247-023-00681-0

Chavez, F. P., & Messié, M. (2009). A comparison of eastern boundary upwelling ecosystems. *Progress in Oceanography*, *83*(1–4), 80–96. https://doi.org/10.1016/j.pocean.2009.07.032

Chen, S. H., Huang, C. C., Kuo, Y. C., Tseng, Y. H., Gu, Y., Earl, K., et al. (2021). Impacts of Saharan mineral dust on air-sea interaction over North Atlantic Ocean using a fully coupled regional model. *Journal of Geophysical Research: Atmospheres*, *126*(4), e2020JD033586. https://doi.org/10.1029/2020JD033586

Chiapello, I., Moulin, C., & Prospero, J. M. (2005). Understanding the long-term variability of African dust transport across the Atlantic as recorded in both Barbados surface concentrations and large-scale Total Ozone mapping spectrometer (TOMS) optical thickness. *Journal of Geophysical Research*, *110*(D18). https://doi.org/10.1029/2004JD005132

Conejero, C., Dewitte, B., Garçon, V., Sudre, J., & Montes, I. (2020). ENSO diversity driving low-frequency change in mesoscale activity off Peru and Chile. *Scientific Reports*, *10*(1), 17902. https://doi.org/10.1038/s41598-020-74762-x

Cropper, T. E., Hanna, E., & Bigg, G. R. (2014). Spatial and temporal seasonal trends in coastal upwelling off Northwest Africa, 1981–2012. *Deep Sea Research Part I: Oceanographic Research Papers*, *86*, 94–111. https://doi.org/10.1016/j.dsr.2014.01.007

Diogoul, N., Brehmer, P., Demarcq, H., El Ayoubi, S., Thiam, A., Sarre, A., et al. (2021). On the robustness of an eastern boundary upwelling ecosystem exposed to multiple stressors. *Scientific Reports*, *11*(1), 1908. https://doi.org/10.1038/s41598-021-81549-1

R. J. H. Dunn, D. M. Stanitski, N. Cobron, & K. M. Willett (Eds.) (2018). *Global climate* (Vol. 99, pp. S5–S68). Bulletin of the American Meteorological Society.

Enfield, D. B., Mestas-Nuñez, A. M., & Trimble, P. J. (2001). The Atlantic multidecadal oscillation and its relation to rainfall and river flows in the continental US. *Geophysical Research Letters*, *28*(10), 2077–2080. https://doi.org/10.1029/2000GL012745

European Commission, Directorate-General for Maritime Affairs and Fisheries, Caillart, B., Cappell, R., & Defaux, V. (2023). *Evaluation and analysis of the sustainable fisheries partnership agreements (SFPAs) between the EU and third countries including an in-depth analysis of the sectoral support component of the SFPAs: Final report*. Publications Office of the European Union. Retrieved from https://data.europa.eu/doi/10.2771/52188

Garçon, V., Dewitte, B., Montes, I., & Goubanova, K. (2019). Land-sea-atmosphere interactions exacerbating ocean deoxygenation in eastern boundary upwelling systems (EBUS). In D. Laffoley & J. M. Baxter (Eds.), *Ocean deoxygenation: Everyone's problem, gland, SWITZ* (pp. 155–170). IUCN.

Georg, T., Neves, M. C., & Relvas, P. (2022). The signature of NAO and EA climate patterns on the vertical structure of the canary current upwelling system. *EGUsphere*, *2022*, 1–14. https://doi.org/10.5194/egusphere-2022-702

Gómez-Gesteira, M., De Castro, M., Álvarez, I., Lorenzo, M. N., Gesteira, J. L. G., & Crespo, A. J. C. (2008). Spatio-temporal upwelling trends along the canary upwelling system (1967–2006). *Annals of the New York Academy of Sciences*, *1146*(1), 320–337. https://doi.org/10.1196/annals.1446.004

Gomez-Gesteira, M., Moreira, C., Alvarez, I., & DeCastro, M. (2006). Ekman transport along the Galician coast (northwest Spain) calculated from forecasted winds. *Journal of Geophysical Research*, *111*(C10). https://doi.org/10.1029/2005jc003331

Gómez-Letona, M., Ramos, A. G., Coca, J., & Arístegui, J. (2017). Trends in primary production in the canary current upwelling System—A regional perspective comparing remote sensing models. *Frontiers in Marine Science*, *4*, 370. https://doi.org/10.3389/fmars.2017.00370

Jacox, M. G., Bograd, S. J., Hazen, E. L., & Fiechter, J. (2015). Sensitivity of the California current nutrient supply to wind, heat, and remote Ocean forcing. *Geophysical Research Letters*, *42*(14), 5950–5957. https://doi.org/10.1002/2015GL065147

Jacox, M. G., & Edwards, C. A. (2011). Effects of stratification and shelf slope on nutrient supply in coastal upwelling regions. *Journal of Geophysical Research*, *116*(C3), C03019. https://doi.org/10.1029/2010JC006547

Jacox, M. G., Edwards, C. A., Hazen, E. L., & Bograd, S. J. (2018). Coastal upwelling revisited: Ekman, Bakun, and improved upwelling indices for the U.S. West Coast. *Journal of Geophyical Research: Oceans*, *123*(10), 7332–7350. https://doi.org/10.1029/2018JC014187

Jing, Z., Wang, S., Wu, L., Wang, H., Zhou, S., Sun, B., et al. (2023). Geostrophic flows control future changes of oceanic eastern boundary upwelling. *Nature Climate Change*, *13*(2), 148–154. https://doi.org/10.1038/s41558-022-01588-y

Kaplan, A., Cane, M. A., Kushnir, Y., Clement, A. C., Blumenthal, M. B., & Rajagopalan, B. (1998). Analyses of global sea surface temperature 1856–1991. *Journal of Geophysical Research*, *103*(C9), 18567–18589. https://doi.org/10.1029/97jc01736

Kessler, A., Goris, N., & Lauvset, S. K. (2022). Observation-based Sea surface temperature trends in Atlantic large marine ecosystems. *Progress in Oceanography*, *208*, 102902. https://doi.org/10.1016/j.pocean.2022.102902

Lentz, S. J., & Chapman, D. C. (2004). The importance of nonlinear cross-shelf momentum flux during wind-driven coastal upwelling. *Journal of Physical Oceanography*, *34*(11), 2444–2457. https://doi.org/10.1175/JPO2644.1

Llope, M., Anadón, R., Sostres, J. Á., & Viesca, L. (2007). Nutrients dynamics in the southern Bay of Biscay (1993–2003): Winter supply, stoichiometry, long-term trends, and their effects on the phytoplankton community. *Journal of Geophysical Research*, *112*(C7). https://doi.org/10.1029/2006JC003573

Mahowald, N. M., Baker, A. R., Bergametti, G., Brooks, N., Duce, R. A., Jickells, T. D., et al. (2005). Atmospheric global dust cycle and iron inputs to the ocean. *Global Biogeochemical Cycles*, *19*(4). https://doi.org/10.1029/2004GB002402

Mann, M. E., Steinman, B. A., Brouillette, D. J., & Miller, S. K. (2021). Multidecadal climate oscillations during the past millennium driven by volcanic forcing. *Science*, *371*(6533), 1014–1019. https://doi.org/10.1126/science.abc5810

Marcello, J., Hernandez-Guerra, A., Eugenio, F., & Fonte, A. (2011). Seasonal and temporal study of the northwest African upwelling system. *International Journal of Remote Sensing*, *32*(7), 1843–1859. https://doi.org/10.1080/01431161003631576

Marrero-Betancort, N., Marcello, J., Rodríguez Esparragón, D., & Hernández-León, S. (2020). Wind variability in the canary current during the last 70 years. *Ocean Science*, *16*(4), 951–963. https://doi.org/10.5194/os-16-951-2020

McGregor, H. V., Dima, M., Fischer, H. W., & Mulitza, S. (2007). Rapid 20th-century increase in coastal upwelling off Northwest Africa. *Science*, *315*(5812), 637–639. https://doi.org/10.1126/science.1134839

Ménard, F., Marsac, F., Bellier, E., & Cazelles, B. (2007). Climatic oscillations and tuna catch rates in the Indian Ocean: A wavelet approach to time series analysis. *Fisheries Oceanography*, *16*(1), 95–104. https://doi.org/10.1111/j.1365-2419.2006.00415.x

Montes, I., Schneider, W., Colas, F., Blanke, B., & Echevin, V. (2011). Subsurface connections in the eastern tropical Pacific during La Niña 1999–2001 and El Niño 2002–2003. *Journal of Geophysical Research*, *116*(C12), C12022. https://doi.org/10.1029/2011JC007624

Narayan, N., Paul, A., Mulitza, S., & Schulz, M. (2010). Trends in coastal upwelling intensity during the late 20th century. *Ocean Science*, *6*(3), 815–823. https://doi.org/10.5194/os-6-815-2010

Pardo, P. C., Padín, X. A., Gilcoto, M., Farina-Busto, L., & Pérez, F. F. (2011). Evolution of upwelling systems coupled to the long-term variability in sea surface temperature and Ekman transport. *Climate Research*, *48*(2), 231–246. https://doi.org/10.3354/cr00989

Pauly, D., & Christensen, V. (1995). Primary production required to sustain global fisheries. *Nature*, *374*(6519), 255–257. https://doi.org/10.1038/374255a0

Pinsky, M. L., Worm, B., Fogarty, M. J., Sarmiento, J. L., & Levin, S. A. (2013). Marine taxa track local climate velocities. *Science*, *341*(6151), 1239–1242. https://doi.org/10.1126/science.1239352

Pitcher, G. C., Aguirre-Velarde, A., Breitburg, D., Cardich, J., Carstensen, J., Conley, D. J., et al. (2021). System controls of coastal and open ocean oxygen depletion. *Progress in Oceanography*, *197*, 102613. https://doi.org/10.1016/j.pocean.2021.102613

Polonsky, A. B., & Serebrennikov, A. N. (2018). Long-term sea surface temperature trends in the Canary upwelling zone and their causes. *Izvestiya, Atmospheric and Oceanic Physics*, *54*(9), 1062–1067. https://doi.org/10.1016/10.1134/S0001433818090281

Rouyer, T., Fromentin, J. M., Ménard, F., Cazelles, B., Briand, K., Pianet, R., et al. (2008). Complex interplays among population dynamics, environmental forcing, and exploitation in fisheries. *Proceedings of the National Academy of Sciences*, *105*(14), 5420–5425. https://doi.org/10.1073/pnas.0709034105

Rykaczewski, R. R., & Dunne, J. P. (2010). Enhanced nutrient supply to the California current ecosystem with global warming and increased stratification in an Earth system model. *Geophysical Research Letters*, *37*(21). https://doi.org/10.1029/2010GL045019

Rykaczewski, R. R., Dunne, J. P., Sydeman, W. J., García-Reyes, M., Black, B. A., & Bograd, S. J. (2015). Poleward displacement of coastal upwelling-favorable winds in the ocean's eastern boundary currents through the 21st century. *Geophysical Research Letters*, *42*(15), 6424–6431. https://doi.org/10.1002/2015GL064694

Seabra, R., Varela, R., Santos, A. M., Gómez-Gesteira, M., Meneghesso, C., Wethey, D. S., & Lima, F. P. (2019). Reduced nearshore warming associated with eastern boundary upwelling systems. *Frontiers in Marine Science*, *6*, 104. https://doi.org/10.3389/fmars.2019.00104

Sousa, M. C., Alvarez, I., de Castro, M., Gomez-Gesteira, M., & Dias, J. M. (2017). Seasonality of coastal upwelling trends under future warming scenarios along the southern limit of the Canary upwelling system. *Progress in Oceanography*, *153*, 16–23. https://doi.org/10.1016/j.pocean.2017.04.002

Sydeman, W. J., García-Reyes, M., Schoeman, D. S., Rykaczewski, R. R., Thompson, S. A., Black, B. A., & Bograd, S. J. (2014). Climate change and wind intensification in coastal upwelling ecosystems. *Science*, *345*(6192), 77–80. https://doi.org/10.1126/science.1251635

Sylla, A., Mignot, J., Capet, X., & Gaye, A. T. (2019). Weakening of the Senegalo–Mauritanian upwelling system under climate change. *Climate Dynamics*, *53*(7), 4447–4473. https://doi.org/10.1007/s00382-019-04797-y

Sylla, A., Sanchez Gomez, E., Mignot, J., & López-Parages, J. (2022). Impact of increased resolution on the representation of the Canary upwelling system in climate models. *Geoscientific Model Development*, *15*(22), 8245–8267. https://doi.org/10.5194/gmd-15-8245-2022

van Hoof, L. (2015). Fisheries management, the ecosystem approach, regionalisation and the elephants in the room. *Marine Policy*, *60*, 20–26. https://doi.org/10.1016/j.marpol.2015.05.011

Varela, R., Lima, F. P., Seabra, R., Meneghesso, C., & Gómez-Gesteira, M. (2018). Coastal warming and wind-driven upwelling: A global analysis. *Science of the Total Environment*, *639*, 1501–1511. https://doi.org/10.1016/j.scitotenv.2018.05.273

Varela, R., Rodríguez-Díaz, L., De Castro, M., & Gómez-Gesteira, M. (2022). Influence of canary upwelling system on coastal SST warming along the 21st century using CMIP6 GCMs. *Global and Planetary Change*, *208*, 103692. https://doi.org/10.1016/j.gloplacha.2021.103692

Vazquez, R., Parras-Berrocal, I., Cabos, W., Sein, D. V., Mañanes, R., & Izquierdo, A. (2022). Assessment of the canary current upwelling system in a regionally coupled climate model. *Climate Dynamics*, *58*(1), 69–85. https://doi.org/10.1007/s00382-021-05890-x

Vázquez, R., Parras-Berrocal, I. M., Cabos, W., Sein, D., Mañanes, R., Bolado-Penagos, M., & Izquierdo, A. (2024). Climate change in the Canary/Iberia upwelling region: The role of ocean stratification and wind. *Environmental Research Letters*, *19*(7), 074064. https://doi.org/10.1088/1748-9326/ad5ab4

Vázquez, R., Parras-Berrocal, I. M., Koseki, S., Cabos, W., Sein, D. V., & Izquierdo, A. (2023). Seasonality of coastal upwelling trends in the Mauritania-Senegalese region under RCP8. 5 Climate change scenario. *Science of the Total Environment*, *898*, 166391. https://doi.org/10.1016/j.scitotenv.2023.166391

Wang, D., Gouhier, T. C., Menge, B. A., & Ganguly, A. R. (2015). Intensification and spatial homogenization of coastal upwelling under climate change. *Nature*, *518*(7539), 390–394. https://doi.org/10.1038/nature14235

Ward, J. H., Jr. (1963). Hierarchical grouping to optimize an objective function. *Journal of the American Statistical Association*, *58*(301), 236–244. https://doi.org/10.2307/2282967

World Meteorological Organization (WMO). (1996). *Climatological Normals (CLINO) for the period 1961-1990, WMO-No. 847*. World Meteorological Organization.

World Meteorological Organization (WMO). (2007). *The role of climatological normals in a changing climate, WMO/TD-No. 1377*. World Meteorological Organization.

World Meteorological Organization (WMO). (2017). *WMO guidelines on the calculation of climate normals, WMO-No. 1203*. World Meteorological Organization.

References From the Supporting Information

Copernicus Climate Change Service (C3S). (2019). ERA5 monthly averaged data on single levels [Dataset]. https://doi.org/10.24381/cds.f17050d7

Copernicus Marine Environment Monitoring Service (CMEMS). (2023a). Global ocean colour Chlorophyll-a concentration L4 [Dataset]. https://doi.org/10.48670/moi-00281

Copernicus Marine Environment Monitoring Service (CMEMS). (2023b). Global ocean sea surface temperature L4 reprocessed [Dataset]. https://doi.org/10.48670/moi-00168

FAO. (2025). FAO major fishing areas. Atlantic, Eastern central (major fishing area 34). CWP data collection. In *Fisheries and aquaculture*. Updated 2004/10/01 [Cited Sunday, December 14th 2025] https://www.fao.org/fishery/en/area/fao:34/en

Gelaro, R., McCary, W., Suarez, M. J., Todling, R., Molod, A., Tackacs, L., et al. (2017). The modern-era retrospective analysis for research and applications, version 2 (MERRA-2) [Dataset]. https://gmao.gsfc.nasa.gov/reanalysis/MERRA-2/

NOAA Climate Prediction Center. (2020). North Atlantic oscillation (NAO) index [Dataset]. Retrieved from https://www.cpc.ncep.noaa.gov/data/teledoc/telecontents.shtml

NOAA Pacific Fisheries Environmental Laboratory. (2021). Bakun upwelling index [Dataset]. Retrieved from https://oceanview.pfeg.noaa.gov/products/upwelling/bakun

NOAA Physical Sciences Laboratory. (2022). Atlantic multidecadal oscillation (AMO) index [Dataset]. Retrieved from https://psl.noaa.gov/data/timeseries/AMO/